Dry active turbulence in microtubule-motor mixtures

Supplemental Material

Ivan Maryshev and Andrew B. Goryachev
Centre for Synthetic and Systems Biology, Institute of Cell Biology, School of Biological Sciences, University of Edinburgh, Max Born Crescent, Edinburgh EH9 3BF, United Kingdom

Davide Marenduzzo and Alexander Morozov
SUPA, School of Physics and Astronomy, The University of Edinburgh, James Clerk Maxwell Building, Peter Guthrie Tait Road, Edinburgh, EH9 3FD, United Kingdom

I. INTERACTION RATES

The interaction functions W defined in the main text determine the rates at which two microtubules (MTs) at $(\mathbf{r}_1, \phi_1)$ and $(\mathbf{r}_2, \phi_2)$ are displaced and reoriented by molecular motors (MMs). In our approach these rates have the following general form:

$$W(\mathbf{r}_1, \phi_1; \mathbf{r}_2, \phi_2) = G \underbrace{\Theta\big(1-|\tau_1|\big)\Theta\big(1-|\tau_2|\big)}_{\text{probability of intersection}} \underbrace{\big\{1+\Xi\big[\Theta(\tau_1-\tau_0)+\Theta(\tau_2-\tau_0)\big]\big\}}_{\text{dependence on the local MM density}}. \tag{S1}$$

The constant G is proportional to the motor properties (e.g., their processivity and the overall density); it varies with the motor type and will be removed from the model by a rescaling, see below. The product of the Heaviside functions gives the geometric probability of two MT intersecting in 2D: since we assume MMs to be rods of negligible thickness, W should be non-zero only when MTs intersect in their original configuration (in other words we do not consider long-range interactions). $\tau_{1,2}$ are the positions of the intersection point along the two MTs. We parametrise these position such that $\tau = 0$ at the MT centre and $\tau = \pm 1$ corresponds to the "+"/"-"-ends, respectively. The expression within the curly brackets depends on the local density of MMs at the intersection point and introduces anisotropy in the interaction, which arises only when $\Xi \neq 0$. τ_0 is the position of the interface between low and high MM density on a particular MT. The derivation of Eq.(S1) is provided in [1].

Eq.(S1) can be written in terms of ξ, ψ, ϕ, and ω as

$$\begin{aligned} W(\mathbf{r}_1, \phi_1; \mathbf{r}_2, \phi_2) =& G\,\Theta\left(|\sin\omega| - \frac{2\xi}{l}|\phi_1-\psi|\right)\Theta\left(|\sin\omega| - \frac{2\xi}{l}|\phi_2-\psi|\right) \\ &\times\left\{1+\Xi\left[\Theta\left(\frac{2\xi}{l}\frac{\sin(\phi_1-\psi)}{\sin\omega}-\tau_0\right)+\Theta\left(\frac{2\xi}{l}\frac{\sin(\phi_2-\psi)}{\sin\omega}-\tau_0\right)\right]\right\}, \end{aligned} \tag{S2}$$

where $\boldsymbol{\xi} = \xi(\cos\psi, \sin\psi) = \mathbf{r}_2 - \mathbf{r}_1$ is the separation vector between MT centres, and $\omega = \phi_2 - \phi_1$ is the angle between their orientations; l is the MT length.

The interaction rates used in the main text read:

$$\begin{aligned} W_1^+ &\equiv W\left(\mathbf{r}-\frac{\boldsymbol{\xi}}{2}, \phi-\frac{\omega}{2}; \mathbf{r}+\frac{\boldsymbol{\xi}}{2}, \phi+\frac{\omega}{2}\right), \\ W_2^+ &\equiv W\left(\mathbf{r}-\frac{\boldsymbol{\xi}}{2}+\frac{\eta l\mathbf{n}}{2}, \phi-\frac{\omega}{2}+\frac{\pi}{2}; \mathbf{r}+\frac{\boldsymbol{\xi}}{2}+\frac{\eta l\mathbf{n}}{2}, \phi+\frac{\omega}{2}+\frac{\pi}{2}\right), \\ W^- &\equiv W(\mathbf{r}, \phi; \mathbf{r}-\boldsymbol{\xi}, \phi-\omega). \end{aligned} \tag{S3}$$

II. FULL MODEL

Using the techniques from Ref. [1], we coarse-grain our microscopic model to arrive at the following equations for the evolution of density (ρ), polar order (p_i), and nematic alignment tensor (Q_{ij}) (this set of equation is referred to

as the "full model" in the main text):

$$\begin{aligned}
\partial_t\rho =&\frac{1}{32}\nabla^2\rho+\frac{\pi}{48}\partial_i\partial_jQ_{ij}+(1+a_3)\,\frac{\pi}{4}\left[-\frac{1}{12\pi^2}\nabla^2\rho^2+\frac{1}{9}\nabla^2Q_{ij}Q_{ij}-\frac{1}{9\pi}\partial_i\partial_j(\rho Q_{ij})\right]\\
&+(1+a_1)\,\frac{\eta^2\pi}{4}\left[\frac{1}{4\pi^2}\nabla^2\rho^2-\frac{1}{3}\nabla^2Q_{ij}Q_{ij}+\frac{1}{2\pi}\partial_i\partial_j(\rho Q_{ij})-2\partial_i\partial_j\left(p_ip_j\right)\right]-\frac{91}{69120\pi}\rho_0\nabla^4\rho, \qquad \text{(S4)}\\
\partial_tp_i =&-p_i+\frac{5}{192}\nabla^2p_i+\frac{1}{96}\partial_i(\partial_kp_k)+(1+a_1)\left[-\frac{3}{11\pi}\rho p_i+\frac{29}{19}Q_{ij}p_j-\frac{7}{18}A_3Q_{kl}Q_{kl}p_i\right]\\
&+a_2\frac{1}{8}\Bigg[-\frac{1}{4\pi^2}\partial_i\rho^2+\left(3p_i(\partial_kp_k)+(p_k\partial_k)p_i-\frac{1}{3}\partial_i(p_kp_k)\right)\\
&\quad-\left(\frac{1}{12\pi}\partial_j(\rho Q_{ij})+\frac{1}{2\pi}Q_{ij}\partial_j\rho\right)+\left(\frac{113}{180}\partial_i(Q_{kl}Q_{kl})-\frac{53}{45}Q_{ij}\partial_kQ_{jk}\right)\Bigg]\\
&+(1+a_3)\,\frac{1}{720}\Bigg[-\frac{31}{\pi}p_i\nabla^2\rho-\frac{6}{\pi}p_k\partial_k\partial_i\rho+\frac{19}{\pi}\left(\rho\nabla^2p_i-\frac{1}{2}\nabla^2(\rho p_i)\right)-61p_i\partial_k\partial_lQ_{kl}\\
&\quad-\frac{7}{\pi}\left((\partial_i\rho)(\partial_kp_k)-\rho\partial_i(\partial_kp_k)+\partial_i(p_k\partial_k\rho)\right)+49(p_k\partial_k)(\partial_jQ_{ij})+31p_k\partial_i\partial_lQ_{kl}+10Q_{kl}\partial_i\partial_kp_l\\
&\quad+28Q_{il}\partial_l(\partial_kp_k)-19Q_{ik}\nabla^2p_k-14\partial_k\partial_l(Q_{kl}p_i)+9\partial_i\partial_k(Q_{kl}p_l)-\frac{9}{2}\nabla^2(Q_{ij}p_j)\Bigg]\\
&+(1+a_1)\,\frac{\eta}{2}\left[\frac{1}{4\pi^2}\nabla\rho^2+\frac{1}{2\pi}\partial_j(\rho Q_{ij})-\frac{1}{3}\partial_iQ_{kl}Q_{kl}-2\partial_j(p_ip_j)\right]\\
&+a_2\frac{\eta}{44}\Bigg[\frac{9}{8\pi}\left(2(p_k\partial_k)\partial_i\rho-2\rho\partial_i(\partial_kp_k)-\rho\nabla^2p_i+p_i\nabla^2\rho\right)+2\left(p_i\partial_k\partial_lQ_{kl}-Q_{kl}\partial_k\partial_lp_i\right)\\
&\quad+\frac{5}{2}((p_k\partial_k)(\partial_jQ_{ij})-Q_{il}\partial_l(\partial_kp_k))+\frac{3}{2}(Q_{kl}\partial_i\partial_kp_l-p_k\partial_i\partial_lQ_{kl})\Bigg], \qquad \text{(S5)}\\
\partial_tQ_{ij} =&-4Q_{ij}+\frac{1}{32}\nabla^2Q_{ij}+\frac{1}{192\pi}\mathcal{D}_{ij}\rho+(1+a_1)\left[\frac{2}{3\pi}\rho Q_{ij}-A_4\frac{6}{5}(Q_{kl}Q_{kl})Q_{ij}\right]\\
&+a_2\left[-\frac{1}{16\pi}\left(\partial_i(\rho p_j)+\partial_j(\rho p_i)-\delta_{ij}\partial_k\left(\rho p_k\right)\right)-\frac{\rho}{24\pi}\left(\partial_ip_j+\partial_jp_i-\delta_{ij}(\partial_kp_k)\right)+\frac{1}{4}Q_{ij}(\partial_kp_k)+\frac{5}{12}(p_k\partial_k)Q_{ij}\right]\\
&+(1+a_3)\,\frac{1}{8}\Bigg[-\frac{1}{36\pi^2}\left(3\left[(\partial_i\rho)(\partial_j\rho)-\frac{\delta_{ij}}{2}(\partial_k\rho)^2\right]+\rho\mathcal{D}_{ij}\rho\right)+\frac{5}{9\pi}\rho\nabla^2Q_{ij}-\frac{1}{3\pi}Q_{ij}\nabla^2\rho-\frac{1}{6\pi}\nabla^2(\rho Q_{ij})\\
&\quad-\frac{11}{45}Q_{ij}\partial_k\partial_lQ_{kl}-\frac{1}{6}\partial_k\partial_l(Q_{ij}Q_{kl})+\frac{7}{15}Q_{kl}\partial_k\partial_lQ_{ij}+\frac{1}{12}\mathcal{D}_{ij}(Q_{kl}Q_{kl})-\frac{1}{5}Q_{kl}\mathcal{D}_{ij}Q_{kl}\Bigg]\\
&+(1+a_1)\,\frac{\eta^2}{8}\left[\frac{1}{4\pi^2}\mathcal{D}_{ij}\rho^2-\partial_i\partial_j(p_kp_k)-2\nabla^2(p_ip_j)-\frac{5}{6}\mathcal{D}_{ij}(Q_{kl}Q_{kl})+\partial_k\partial_l(Q_{kl}Q_{ij})+\frac{1}{2\pi}\nabla^2(\rho Q_{ij})\right]. \qquad \text{(S6)}
\end{aligned}$$

These equations were rendered dimensionless by scaling time, space and the Fourier harmonics of P by D_r^{-1}, L and GL^2/D_r, respectively; the indices refer to the two-dimensional Cartesian components and the Einstein summation convention is employed; $\nabla^2=\partial_k\partial_k$, and we introduced the operator $\mathcal{D}_{ij}=\partial_i\partial_j-\frac{\delta_{ij}}{2}\partial_k\partial_k$. Note, that these equations can be written in a more compact form in terms of complex fields and the Wirtinger derivatives $\underline{\nabla}=\partial_x+i\partial_y$ and $\underline{\nabla}^*=\partial_x-i\partial_y$, where * denotes complex conjugation. However, we find the resulting equations more difficult to read and prefer to keep the original notation.

Coefficients A_3 and A_4 are coming from the adiabatic elimination of higher Fourier modes of $P(\mathbf{r},\phi)$; for the details of the closure procedure see [1]. Their expressions are given by:

$$A_4=3\left(\frac{1}{1+a_1}+\frac{\rho_0}{5\pi}\right)^{-1},\quad A_3=\left(\frac{15}{8}\frac{1}{1+a_1}+\frac{19\rho_0}{48\pi}\right)^{-1}. \qquad \text{(S7)}$$

Finally, we have also introduced the following quantities that depend on Ξ and τ_0:

$$a_1 = \Xi\left(1-\tau_0\right), \qquad a_2 = \Xi\left(1-\tau_0^2\right), \qquad a_3 = \Xi\left(1-\tau_0\left(1+\tau_0^2\right)/2\right). \tag{S8}$$

III. MINIMAL MODEL

As discussed in the main text, as a first step in deriving a minimal model, we use our observation that the polar order plays only a minor role in the simulations of the full model. By keeping only the lowest order terms in spatial gradients in Eq. (S5), we can adiabatically eliminate p_i from the other equations by replacing it with

$$p_i = \frac{\rho_0}{1+(1+a_1)\frac{3}{11\pi}\rho_0}\left[\left(\frac{1+a_1}{4\pi^2}\eta - \frac{a_2}{16\pi^2}\right)\partial_i\rho + \left(\frac{1+a_1}{4\pi}\eta - \frac{a_2}{96\pi}\right)\partial_j Q_{ij}\right]. \tag{S9}$$

This procedure resulted in two dynamical equations for ρ and Q_{ij}. We then systematically switched off each term individually in these equations, and computed the resulting phase diagram in each case. The term was reinstated only if it significantly changed the position of the phase boundary, as compared with the phase diagram of the full model. By following this procedure, we obtained the following minimal model

$$\partial_t\rho = \nabla^2\left[\frac{1}{32}\rho + \mu\rho^2\right] + \partial_i\partial_j\left[\frac{\pi}{48} + \chi\rho\right]Q_{ij} - \lambda\nabla^2\left(Q_{kl}Q_{kl}\right), \tag{S10}$$

$$\partial_t Q_{ij} = \left[4\left(\rho/\rho_{cr}-1\right) - \alpha Q_{kl}Q_{kl} + \kappa\nabla^2\right]Q_{ij} + \zeta\mathcal{D}_{ij}\rho - \beta_1\mathcal{D}_{ij}\left(Q_{kl}Q_{kl}\right) - \beta_2 Q_{kl}\mathcal{D}_{ij}Q_{kl}, \tag{S11}$$

where the parameters are given by

$$\begin{aligned}
\mu =& \frac{1+a_1}{16\pi}\eta^2 - \frac{1+a_3}{48\pi}, \quad \chi = \frac{1+a_1}{8}\eta^2 - \frac{1+a_3}{36}, \quad \lambda = \pi\left(\frac{1+a_1}{12}\eta^2 - \frac{1+a_3}{36}\right), \quad \alpha = \frac{2(1+a_1)}{\frac{5}{1+a_1}+\frac{\rho_0}{\pi}},\\
\kappa =& \frac{1}{32} + \left(\frac{1+a_1}{16\pi}\eta^2 + \frac{7(1+a_3)}{144\pi}\right)\rho_0 - \frac{5a_2}{48\pi\left(1+(1+a_1)\frac{3}{11\pi}\rho_0\right)}\left(\frac{1+a_1}{4\pi}\eta - \frac{a_2}{96\pi}\right)\rho_0^2,\\
\zeta =& \frac{1}{192\pi} + \left(\frac{1+a_1}{16\pi^2}\eta - \frac{1+a_3}{288\pi^2}\right)\rho_0 - \frac{5a_2}{24\pi\left(1+(1+a_1)\frac{3}{11\pi}\rho_0\right)}\left(\frac{1+a_1}{4\pi^2}\eta - \frac{a_2}{16\pi^2}\right)\rho_0^2,\\
\beta_1 =& \frac{5\eta^2(1+a_1)}{48} - \frac{1+a_3}{96}, \qquad \beta_2 = \frac{1+a_3}{40}, \qquad \rho_{cr} = \frac{6\pi}{1+a_1}.
\end{aligned} \tag{S12}$$

We note here that the minimal equations presented above cannot be derived from the full model using the amplitude-equation-like techniques where only terms up to a particular order in the distance to an instability threshold are preserved. Application of such techniques to our full model results in a model with a smaller number of terms than the minimal one presented above, and, as has already been noted, all the terms in our minimal model are required to reproduce the phase behaviour of the full system of equations.

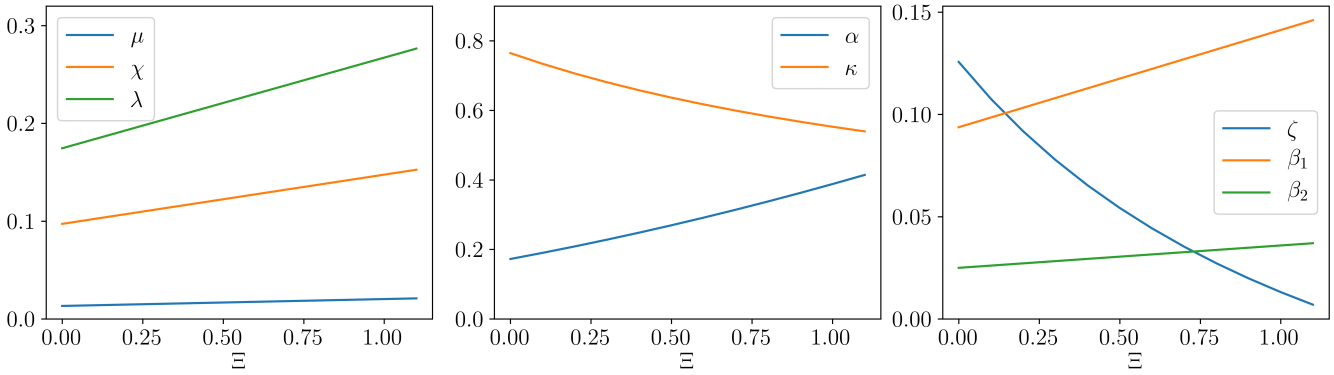

FIG. S1: Dependence of the minimal model parameters on Ξ ($\rho_0 = 1.1\rho_{cr}, \tau_0 = 0.5$).

IV. LINEAR STABILITY ANALYSIS

Here we perform a linear stability analysis of the minimal model, Eqs. (S10) and (S11). Without loss of generality, we assume that the base state has a uniform density ρ_0 and a uniform nematic order of strength Q_0, oriented along the x-direction. We introduce infinitesimal perturbations to the ρ and Q_{ij} fields

$$\begin{aligned}\rho(\mathbf{r},t) &= \rho_0 + \delta\rho e^{i\mathbf{k}\cdot\mathbf{r}} e^{\hat{\sigma}t},\\ Q_{xx}(\mathbf{r},t) &= Q_0 + \delta Q_{xx} e^{i\mathbf{k}\cdot\mathbf{r}} e^{\hat{\sigma}t},\\ Q_{xy}(\mathbf{r},t) &= \delta Q_{xy} e^{i\mathbf{k}\cdot\mathbf{r}} e^{\hat{\sigma}t},\end{aligned} \tag{S13}$$

where k_x and k_y set the lengthscale of the perturbation, and $\hat{\sigma}$ is a temporal eigenvalue. We substitute these expressions into Eqs.(S10) and (S11), and linearise the resulting equations with respect to the perturbations to obtain

$$\hat{\sigma}\begin{pmatrix}\delta\rho\\ \delta Q_{xx}\\ \delta Q_{xy}\end{pmatrix} = \begin{pmatrix}-(1/32+2\mu\rho_0)k^2 - \chi Q_0\bar{k}^2 & -(\pi/48+\chi\rho_0)\bar{k}^2 + 4Q_0\lambda k^2 & -(\pi/24+2\chi\rho_0)k_xk_y\\ 4Q_0/\rho_{cr} - \zeta\bar{k}^2/2 & 4\left(\rho_0/\rho_{cr}-1\right) - 6\alpha Q_0^2 + (2\beta_1+\beta_2)Q_0\bar{k}^2 - \kappa k^2 & 0\\ -\zeta k_xk_y & 2(2\beta_1+\beta_2)Q_0k_xk_y & 4\left(\rho_0/\rho_{cr}-1\right) - 2\alpha Q_0^2 - \kappa k^2\end{pmatrix}\begin{pmatrix}\delta\rho\\ \delta Q_{xx}\\ \delta Q_{xy}\end{pmatrix}, \tag{S14}$$

where $k^2 = k_x^2 + k_y^2$, and $\bar{k}^2 = k_x^2 - k_y^2$. We proceed by studying the linear stability of various base states.

A. Stability of the Homogeneous and Isotropic State

Linear stability of the homogeneous and isotropic state is determined by the eigenvalue problem, Eq.(S14) with $Q_0 = 0$. Explicitly solving the eigenvalue problem, yields

$$\hat{\sigma} = 4\left(\rho_0/\rho_{cr} - 1\right) - \kappa k^2 \tag{S15}$$

for the most unstable eigenvalue. The instability sets in at $k = 0$ and $\rho_0 = \rho_{cr}$, corresponding to the transition to a globally-ordered nematic state (see Fig. S2 a).

B. Linear Stability of the Nematic State

For $\rho_0 > \rho_{cr}$, the homogeneous and isotropic state is unstable towards the formation of a global nematic phase with the amplitude Q_0, given by the spatially-independent terms in Eq.(S11)

$$Q_0 = \sqrt{\frac{2}{\alpha}\left(\frac{\rho_0}{\rho_{cr}} - 1\right)}. \tag{S16}$$

Using this value in Eq.(S14) yields an eigenvalue problem that is too complicated to analyse analytically, and, instead, we study it numerically using Wolfram Mathematica. First, we observe that the globally oriented nematic state is always linearly unstable for $\rho_{cr} < \rho_0 < \rho_N$ (i.e., the region between the blue and orange lines in Fig. S2 b), where the upper phase boundary ρ_N is determined numerically. The most unstable perturbations correspond to $k_x = 0$, with the eigenvector in the form $(\delta\rho, \delta Q_{xx}, 0)$. This instability results in the modulation of the density and nematic order in the direction perpendicular to the nematic direction, and indicates the formation of the nematic bands, discussed in the main text.

C. Second Linear Instability of the Nematic State

As discussed in the main text, for densities significantly larger that ρ_{cr}, there exists another linear instability of the global nematic state, which is different from the one discussed above. Numerical analysis shows that the corresponding eigenvector has a significant δQ_{xx} component, and a very small density modulation $\delta\rho$. To get an insight into the

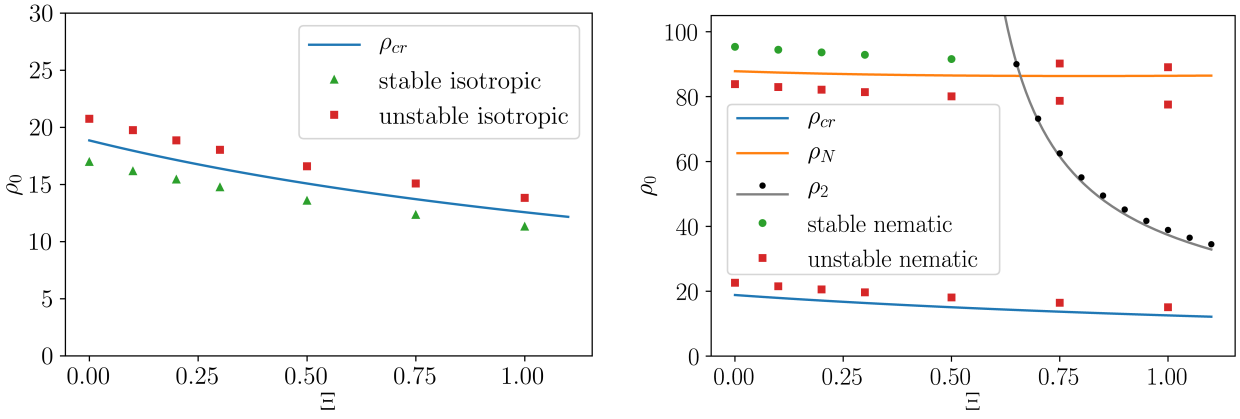

(a) Isotropic state

(b) Nematic state

FIG. S2: Liner stability of the minimal model. (a) Stability of the homogeneous isotropic state, green triangles and red squares represent stable and unstable solutions obtained in the numerical simulations. (b) Stability of the nematic phase. The region between the blue and orange lines is unstable to phase separation; the region above the black dots denote the second instability described in the text (the gray line is the analytical approximation for this instability based on Eq. (S17)). Green circles and red squares represent stable and unstable solutions obtained in the numerical simulations. For both cases $\eta = 1$ and $\tau_0 = 0.5$.

nature of this instability, we set $\delta\rho$ to zero in Eq.(S14) to obtain a simple problem with the most unstable eigenvalue given by

$$\hat{\sigma} = 4\,(\rho_0/\rho_{cr} - 1) - 6\alpha Q_0^2 + (2\beta_1 + \beta_2)Q_0\bar{k}^2 - \kappa k^2. \tag{S17}$$

For all the values of parameters discussed in this work, the coefficient in front of k_y^2 is always negative, and we conclude that the most unstable eigenvalue corresponds to $k_y = 0$. This eigenvalue becomes positive when $(2\beta_1 + \beta_2)Q_0 > \kappa$. For the parameters used in our analysis, $\eta = 1$ and $\tau_0 = 1/2$, this condition can be satisfied for $\Xi > 0.49$, and the corresponding densities above which the instability arises are given in Fig. S2 b as black circles (the analytical approximation for the instability boundary, Eq. (S17), is shown as a gray line). As Eq. (S17) suggests, our minimal model does not predict a selected lengthscale for this instability due to the lack of higher-order spatial gradients in Eqs. (S10) and (S11), and, instead, the fastest growth is observed at the smallest scale available. This instability exists only for relatively large values of Ξ and ρ_0 and is superseded by the main instability discussed above and in the main text.

V. COARSENING

As was mentioned in the main text, in the case where the interaction rates are isotropic ($\Xi = 0$), nematic domains undergo a coarsening process and tend to form one band in steady state.

To characterise the way in which domains coarsen, we here quantify how the typical domain length scale ℓ grows with time. First, we compute the structure factor, $S = \langle\rho(t, \mathbf{k})\rho(t, -\mathbf{k})\rangle$, by averaging the output of the simulation at late times. Then, we define ℓ as

$$\ell(t) = 2\pi\frac{\int S(\mathbf{k}, t)d\mathbf{k}}{\int kS(\mathbf{k}, t)d\mathbf{k}}, \tag{S18}$$

where $k = |\mathbf{k}|$. Simulations to compute ℓ as a function of time t are initialised with a system with uniform density and nematic order, with a small amount of noise.

After a brief transient (not shown) we observe that the length scale ℓ of nematic domains grows as $\ell \sim t^\theta$, where $\theta \approx 0.25$ (Fig. S3), in line with numerical results obtained for growth of passive nematic droplets [2]. We note that the value of the exponent is also numerically close to the one observed for the growth of droplets of spherical self-propelled particles in motility-induced phase separation [3].

In the regime where we observe dry active turbulence, domains transiently coarsen to form one or few bands, however they undergo subsequent instabilities according to the mechanism described in the main text.

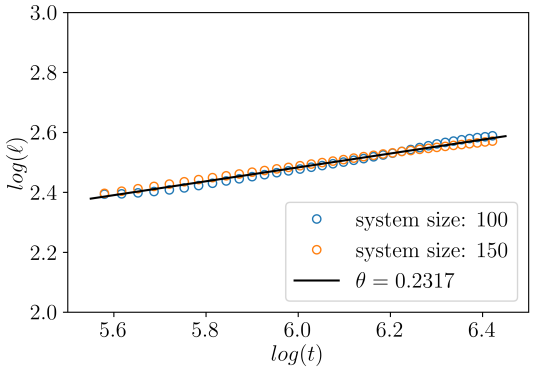

FIG. S3: Plot of the characteristic lengthscale ℓ as a function of time. Blue and orange circles are numerical result corresponding the systems of different size (minimal model, $\Xi = 0$, $\rho_0 = 1.1\rho_{cr}$); the solid line is the power-law fit $\ell \sim t^{\theta}$.

VI. CAPTIONS FOR SUPPLEMENTARY MOVIES

Suppl. Movie 1. Movie showing the simulation results for the evolution of density and nematic ordering in the full model, with $\Xi = 0$, and $\rho_0 = 20.735$. System size: 50×50; $dx = 0.5$, $dt = 0.005$. The movie illustrates formation of a single steady state band in the case of isotropic interaction rates.

Suppl. Movie 2. Movie showing the simulation results for the evolution of density and nematic ordering in the full model, with $\Xi = 0.1$, $\tau_0 = 0.5$, and $\rho_0 = 19.747$. System size: 150×150; $dx = 0.5$, $dt = 0.005$. The movie illustrates the dry active turbulence regime and corresponds to Figure 2b of the main text.

Suppl. Movie 3. Movie showing the simulation results for the evolution of density and nematic ordering in the full model, with $\Xi = 0.1$, $\tau_0 = 0.5$, $\rho_0 = 19.747$. System size: 50×50; $dx = 0.5$, $dt = 0.005$. The movie illustrates the mechanism of band disruption and reformation in the dry active turbulence regime and corresponds to Figure 2c of the main text.

Suppl. Movie 4. Movie showing the simulation results for the evolution of density and nematic ordering in the minimal model, with $\Xi = 0$, $\rho_0 = 20.735$. System size: 50×50; $dx = 0.5$, $dt = 0.005$. The movie illustrates formation of a single steady state band in the case of isotropic interaction rates in the minimal model.

Suppl. Movie 5. Movie showing the simulation results for the evolution of density and nematic ordering in the minimal model, with $\Xi = 0.1$, $\tau_0 = 0.5$, $\rho_0 = 19.747$. System size: 50×50; $dx = 0.5$, $dt = 0.005$. The movie illustrates the dry active turbulence in the minimal model and corresponds to Figure 3a of the main text.

Suppl. Movie 6. Movie showing the simulation results for the evolution of density and nematic ordering in the minimal model, with $\Xi = 0.3$, $\tau_0 = 0.5$, $\rho_0 = 18.03$. System size: 150×150; $dx = 0.5$, $dt = 0.005$. The movie illustrates the dry active turbulence in the minimal model in a large system and corresponds to Figure 3b of the main text.

Suppl. Movie 7. Movie showing the simulations results for the evolution of density and nematic ordering in the modified minimal model in which β_1, β_2 , and ζ are equal to zero ($\Xi = 0$, $\rho_0 = 20.735$; system size: 50×50; $dx = 0.5$, $dt = 0.005$). The movie illustrates the mechanism of band formation and corresponds to Figure 3c of the main text.

Suppl. Movie 8. Movie showing the simulations results for the evolution of density and nematic ordering in the modified minimal model in which χ is equal to zero ($\Xi = 0$, $\rho_0 = 20.735$; system size: 50×50; $dx = 0.5$, $dt = 0.005$). The movie illustrates the role of χ.

Suppl. Movie 9. Movie showing the simulations results for the evolution of density and nematic ordering in the modified minimal model in which parameter ζ is equal to zero ($\Xi = 0$, $\rho_0 = 20.735$; system size: 50×50; $dx = 0.5$, $dt = 0.005$). The movie illustrates the dry active turbulence regime with $\zeta = 0$ and corresponds to Figure 3d of the main text.

Suppl. Movie 10. Movie showing the simulations results for the evolution of density and nematic ordering in the modified minimal model in which β_1 and β_2 are equal to zero ($\Xi = 0$, $\rho_0 = 20.735$; system size: 50×50; $dx = 0.5$, $dt = 0.005$). The movie illustrates band undulation and corresponds to Figure 3e of the main text.

Suppl. Movie 11. Movie showing the simulations results for the evolution of density and nematic ordering in the modified minimal model in which β_1 and β_2 are equal to zero while ζ is multiplied by 1.1 ($\Xi = 0$, $\rho_0 = 20.735$; system size: 50×50; $dx = 0.5$, $dt = 0.005$). The movie illustrates a pathway to chaotic dynamics based on band undulations.

Suppl. Movie 12. Movie showing the simulations results for the evolution of density and nematic ordering in the modified minimal model in which β_1 and β_2 are equal to zero while ζ is multiplied by 1.5 ($\Xi = 0$, $\rho_0 = 20.735$; system size: 50×50; $dx = 0.5$, $dt = 0.005$). The movie illustrates a similar pathway to chaotic dynamics as in Suppl. Movie 11.

---

[1] I. Maryshev, D. Marenduzzo, A. B. Goryachev, and A. Morozov, Phys. Rev. E **97**, 022412 (2018).
[2] M. Mata, C. J. García-Cervera, and H. D. Ceniceros, J. Non-Newtonian Fluid Mech. **212**, 18 (2014).
[3] J. Stenhammar, A. Tiribocchi, R. J. Allen, D. Marenduzzo, and M. E. Cates, Phys. Rev. Lett. **111**, 145702 (2013).